Article ID: 1006-8775(2016) 01-0083-11

CHARACTERISTICS OF BOUNDARY LAYER AND ITS EFFECTS ON ATMOSPHERIC AEROSOL CONCENTRATIONS IN DONGGUAN, GUANGDONG

XIA Dong (夏 冬)[1], FAN Shao-jia (范绍佳)[2], LIAO Zhi-heng (廖志恒)[2]
(1. Dongguan Meteorological Observatory, Dongguan, Guangdong 523086 China; 2. School of Environmental Science and Engineering, Sun Yat Sen University, Guangzhou 510275 China)

Abstract: The structure of atmospheric boundary layer determines the ability of atmospheric dispersion and has an essential impact on airborne aerosols. In this paper, the data of a radio sounding experiment held in Dongguan National Meteorological Observation Station, which is in a coastal city in Pearl River Delta, as well as the data of atmospheric aerosols, were utilized in order to analyze the characteristics of atmospheric boundary layer and its effects on surface aerosol concentrations. The results are showed at follows: the local circulations, associated with dominant winds, made complex structures of atmospheric layers, as the cold air and systematic winds weakened in the end of a cold air event. Weakened wind shears and inversion layers, especially a strong near-surface inversion layer, remarkably diminished the atmospheric diffusion abilities and facilitated an especially high concentration of surface aerosols. The convergence line or weak shear line of sea breeze in the ground level helps weaken the atmospheric diffusion abilities and results in atmospheric aerosols accumulation.

Key words: boundary layer characteristics; aerosol concentration; radio sounding; Dongguan
CLC number: P412.23 **Document code:** A
doi: 10.16555/j.1006-8775.2016.01.010

1 INTRODUCTION

According to Chan et al.[1] and Wu et al.[2], air pollution, especially fine particulate pollution, is a significant problem affecting cities in the Pearl River Delta (PRD). Large-scale adverse weather systems, such as tropical cyclone periphery downdraft, may result in high particulate matter concentration and atmospheric pollution in PRD (Chen et al.[3]). In summer or autumn, tropical cyclone periphery downdraft holds down the height of the atmospheric boundary layer, slows surface atmospheric motion, and thus restricts the convection or diffusion of atmospheric aerosols (Feng et al.[4]; Wu et al.[5]; Xia et al.[6]). Local circulation, such as land and sea breeze or heat island circulation, may also intensify or directly result in pollution incidents (Ding et al.[7]; Fan et al.[8]). Furthermore long-distance transportation or pollutants may also play a significant role in the air pollution of PRD cities (Ding et al.[9]; Xiao et al.[10]).

Received 2014-10-31; **Revised** 2015-09-29; **Accepted** 2016-01-15
Foundation item: National Natural science foundation of China (41205123); National Basic Research Program (2011CB403403); Southern China Regional Meteorological Center Science and Technology Project (GRMC2014Z03); Science and Technology Innovation Team Plan of Guangdong Meteorological Bureau (201103)
Biography: XIA Dong, Ph.D., Associate Professor, primarily undertaking research on atmospheric physics and environment.
Corresponding author: XIA Dong, e-mail: 584131440@163.com

The atmospheric boundary layer is a significant impact factor on near-surface atmospheric pollutant dispersion. According to many studies, meteorological processes on the boundary layer may significantly affect the duration of atmospheric pollution and the spatial scale of pollutant dispersion (Carreras and Pignata[11]; Cogliani[12]; Khedairia and Khadir[13]; Tan et al.[14]; Menut et al.[15]; Grinn-Gofron[16]). Wind direction, wind speed and boundary layer height are the key factors (Kolev et al.[17]) affecting atmospheric pollutant dispersion and transport, and horizontal transport of pollutants from surrounding areas has significant impacts on urban air quality (Davies[18]; Gao et al.[19]; Schleicher et al.[20]). Compared to boundary layer radar observation and other modern remote-sensing monitoring methods, sounding balloon observation is the most direct and feasible method for obtaining data on boundary layer structure (Zhang et al.[21]; Neff et al.[22]; Hanna et al.[23]; Emeis et al.[24]). A large amount of sounding balloon observation data showed that a minor static wind and a thermal inversion layer at the bottom of the troposphere are the significant reasons causing atmospheric pollution (Alappattu and Kunhikrishnan[25]; Kolev et al.[17]).

This paper, by using the atmospheric boundary layer wind and temperature profile data obtained by a sounding balloon from the Dongguan National Basic Meteorological Station (see Fig.1 for the geographic location) in January 2014, as well as the observation data related to atmospheric aerosol concentration, visibility and routine meteorological elements (wind direction,

wind force, temperature, air pressure and humidity) from automatic meteorological stations, analyzed and studied Dongguan's boundary layer structure and its impact on atmospheric aerosol concentration.

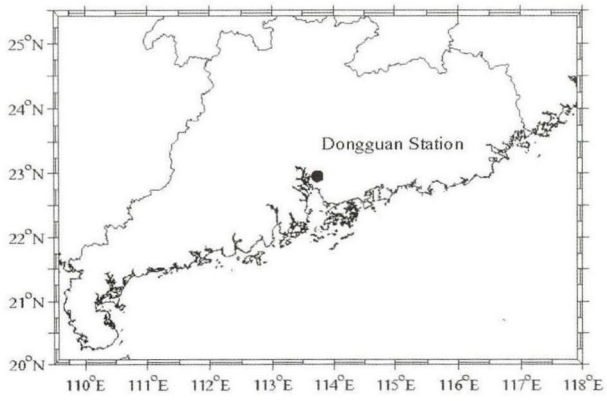

Figure 1. Location of Dongguan Observatory,

2 DATA AND METHODS

The theodolite used in the observations described above was the GYR1 electronic optical pilot balloon theodolite developed and produced by Nanjing Zhong Huatong Electric Co., Ltd. When making midair wind observations, the observatory needs to track the balloon manually, and the theodolite can measure the azimuthal angle and elevation angle of the balloon automatically and regularly; the azimuthal angle and elevation angle observed by the theodolite can be transferred to the computer via the communication interface; and the computer can use a theodolite data processing software to calculate the direction and speed of wind at different altitudes. The sonde used was the single-temperature sonde produced by the Department of Physics of Peking University; the receiver used was the supporting receiver developed and produced by the Peking University and Inner Mongolia Automatons Region Meteorological Science Research Institute. The experiment was performed with eight sounding observations a day, respectively at 6:00, 8:00, 10:00, 14:00, 16:00, 18:00, 20:00 and 23:00 (Local Time). With the temperature observation results obtained by the temperature sonde carried by the sounding balloon and the balloon heights measured by the double theodolites at different times, the temperature at different heights can be obtained. Through the baseline wind observation and low-altitude sounding observation, the wind direction, wind speed and temperature profile at different heights within three kilometers in the near-surface atmospheric layer during the observation period can be obtained.

The Dongguan Banling National Basic Meteorological Station (No.59289) is located in Botanic Garden in the Nancheng District of Dongguan, with green plants in the surrounding 1 kilometer. These are mainly the fruit trees, garden plants and grass. The observed data are well representative. The particulate matter monitor (Grimm 180, GRIMM Aerosol Technik GmbH & CO. KG) and forward-scatter visibility meter (USA Belfore M6000 type) were installed in the Dongguan Banling National Basic Meteorological Station. The Grimm 180 particulate matter monitor measured particulate matter by using the scattering light technique, and measured particulate matter with diameters from 0.25 to 32 μm through 31 channels. Based on the particle density hypothesis, PM_{10}, $PM_{2.5}$ and PM_1 mass concentration can be calculated. The forward-scatter visibility meter measured the scattering coefficient based on the forward-scattering principle of particulate matter for light. The visibility can be calculated using the corresponding relationship of light extinction coefficient and visibility. The original resolution data of the visibility meter is 1 min. The meteorological elements could be obtained through the automatic meteorological stations. After performing aberrant point removal for all of the above original data, the corresponding hourly average could be obtained, which could be used for the analysis in this paper. All observation instruments were inspected and calibrated on a regular basis according to the standard operating procedures.

3 WEATHER BACKGROUND

3.1 *Change characteristics of weather situation and meteorological elements*

Dongguan is located in the eastern central PRD region, with significant tropical monsoon climate. In the winter half of the year, due to the mainland cold high-pressure ridge control, there is a dominant northeasterly wind; in the summer half of the year, there is dominant southwest wind and southeast wind, and frequent high temperatures and rainy weather. In winter or spring, at the end of or after cold air influence, the cold high-pressure ridge deforms and weakens, stabilizing the weather; however, as the wind force weakens, continuous dust-haze weather easily occurs.

Figure 2 shows the changes in the sea-level pressure and the 500 hPa geopotential height on 5-7 January, 2014. Fig.3 shows the changes in the wind direction, wind speed, air temperature, relative humidity and air pressure at the Dongguan Meteorological Station on 5-7 January, 2014. On 5 January, 2014, due to the supplemental impact of weak cold air, the air temperature of the PRD region decreased. According to Fig.2, the PRD region was apparently controlled by a cold high-pressure ridge at 08:00, sea-level pressure in Dongguan was between the 1 020 and 1 022.5 surface isopiestic line; the cold high-pressure ridge was still present on 6 January, but its strength decreased and the air pressure reduced gradually (Fig.3). By 7 January, the cold high-pressure ridge weakened significantly. However, a 500-hPa contour line was rather straight in southern China and there was no obvious weather system affecting Dongguan. Under the control of the cold

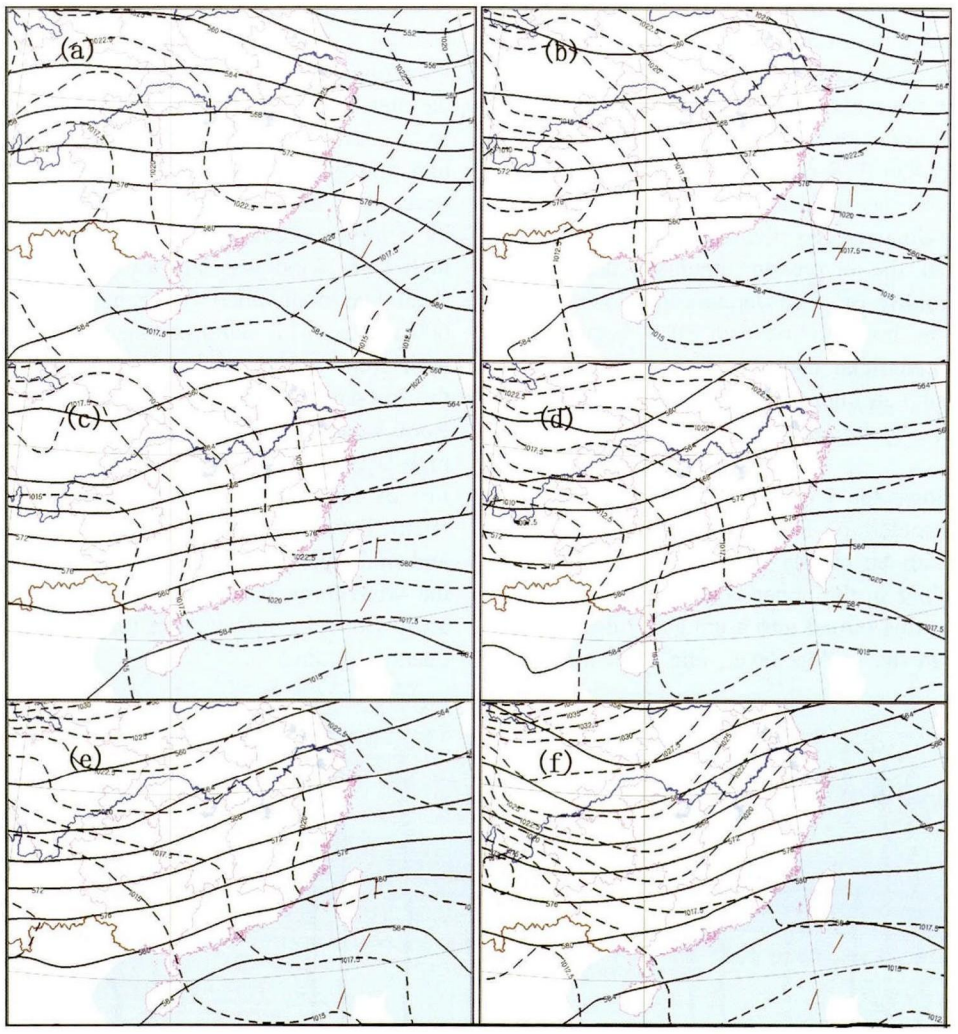

Figure 2. Variations of sea surface pressure and 500 hPa geopotential height (a) 8:00 on 5 January 2014 (b) 20:00 on 5 January 2014 (c) 8:00 on 6 January 2014 (d) 20:00 on 6 January 2014 (e) 8:00 on 7 January 2014 (f) 20:00 on 7 January 2014.

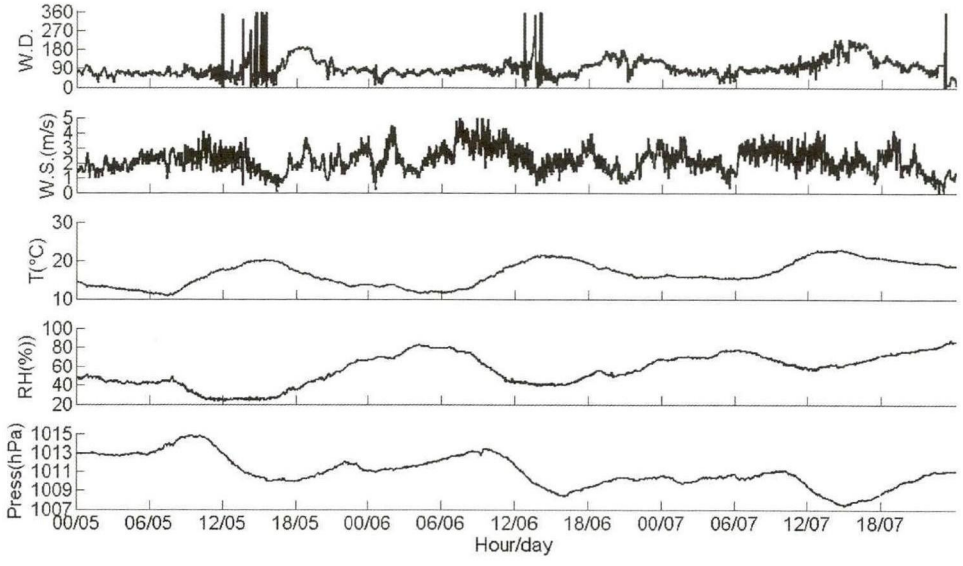

Figure 3. Variations of wind direction, wind speed, temperature, relative humidity and press from 5 to 7, January 2014 at Dongguan observatory.

high-pressure ridge, sunny weather was dominant on 5–7 January, though it was comparatively dry. The minimum temperature in the early morning of 5 January was almost 10℃, but the maximum temperature in the daytime rose to 20℃ or above; the temperature difference was almost 10℃. On 6–7 January, the air temperature rose slowly, but the day-night air temperature difference was 10℃ approximately. As the impact of mainland cold air weakened, the air pressure gradually decreased. The relative humidity on 5–7 January rose gradually. The humidity was, however, beneath 80% most of the time, being not beneficial for aerosol moisture absorption growth, which can intensify visibility deterioration.

3.2 *Characteristics of atmospheric boundary layer structure*

Figure 4 shows the wind varying with the height from 0 to 2 500 meters on 5–7 January, 2014. According to Fig.4, it can be clearly seen that the southwest wind was prevailing in the lower layer at 6:00–8:00 on May 5, 2014, but this turned into a gradually decreasing northwest wind in the middle layer, and even a southeast wind in the higher layer. At 10:00, the wind at the bottom of the boundary layer obviously weakened, but the stronger W-NW-ward wind was stronger in the middle and lower layer. From 12:00, the wind in the whole layer weakened significantly, and the wind at the bottom and middle layer of the boundary layer was very weak. The lower layer wind increased from 20:00 and by a larger extent at 23:00. However, the middle and high layer wind was still weak, and an apparent wind shear was maintained at the height of approximately 1 000 meters. This wind profile structure was maintained until 10:00 on 6 January. At 14:00–16:00 on 6 January, the low-layer wind force weakened, but the difference from 5 January was the apparent increase of mid- and high-layer wind. The change in the wind profile structure of the boundary layer on 7 January was very similar to that of 6 January; however the wind in the high- and mid-layer was larger. After 14:00 on 7 January, as the wind force was too great and the balloon flew far away from the information receiver, the data is subsequently missing.

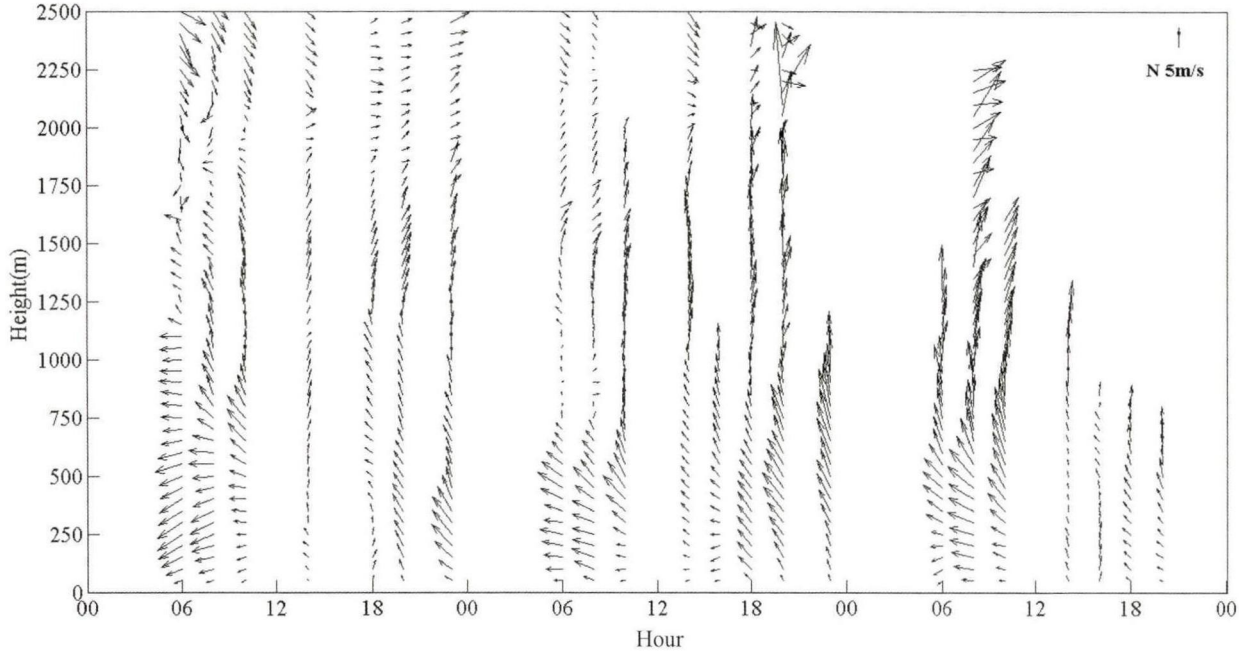

Figure 4. Vertical wind profiles from 5 to 7, January 2014 at Dongguan observatory.

It can be seen that the wind profile structure at the bottom of the boundary layer has comparatively significant daily change characteristics. However the daily changes in the high layer are not apparent, because the low boundary layer tends to be affected by local circulation, but the top boundary layer is mostly affected by weather systems.

Figure 5 shows the change characteristics of the temperature profile on 5–7 January, 2014. It shows that the temperature profiles of these three days (5–7 January) had multilayer characteristics, especially in the early morning. At this time, two to three thermal inversion layers occurred at heights varying from the ground surface to 2 500 m, for example the weak thermal inversion layer or uniform-temperature layer occurring at a height lower than 1 000 m at 6:00 to 8:00 on 5 January. Air temperature above 1 000 m decreased gradually as the height increased, but a weak thermal inversion layer occurred at the high layer. A stronger ground thermal inversion layer occurred at a height lower than 500 m at 6:00 to 8:00 on 6 January, where the temperature difference between the ground surface and 500 m

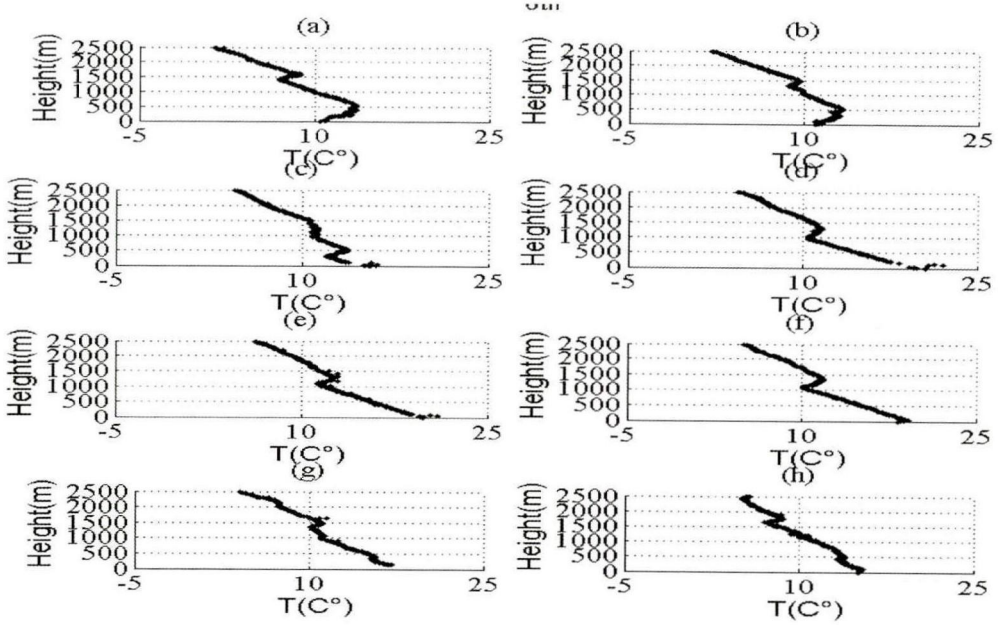

Figure 5. Temperature profiles from 5 to 7, January 2014 at Dongguan observatory. (a) 6:00; (b) 8:00; (c) 10:00; (d) 14:00; (e) 16:00; (f) 18:00; (g) 20:00; (h) 23:00.

was 5℃ or above. Meanwhile, a thermal inversion layer occurred at the height of 1 500 m approximately. On 7 January, weak ground thermal inversion layers occurred only at the height of 500 to 1 000 m. During the day of 5 January, the thermal inversion layer weakened gradually after 10:00, and a weak ground thermal inversion layer occurred at the bottom boundary layer after 18:00. During the day of 6 January, the thermal inversion layer below 500 m disappeared gradually after 10:00, but a thermal inversion was maintained at the middle and high layer. On 7 January, no thermal inversion layer existed.

4 RESULTS AND ANALYSIS

4.1 *Impact of boundary layer on aerosol concentration*

Figure 6 shows the change tendency of PM_{10}, $PM_{2.5}$ and PM_1, as well as atmospheric visibility in Dongguan on 5–7 January, 2014. According to Fig.6, taking $PM_{2.5}$ concentration as an example, aerosol concentration in the early morning of 5 January was approximately 100 $\mu g \cdot m^{-3}$, but then decreased to 70 $\mu g \cdot m^{-3}$ at 12:00; whereas aerosol concentration rose rapidly after 12:00 and reached 130 $\mu g \cdot m^{-3}$ at 18:00, and then further rose interruptedly afterwards and reached a peak of 150 $\mu g \cdot m^{-3}$, which was almost 100% higher than at 12:00 of 5 January. Such a high concentration lasted until 10:00 on 6 January, but decreased rapidly from 18:00 on 7 January and even fell to a minimum 50 $\mu g \cdot m^{-3}$ or below. The change in visibility was opposite to that of aerosol concentration. Relative humidity was mostly lower than

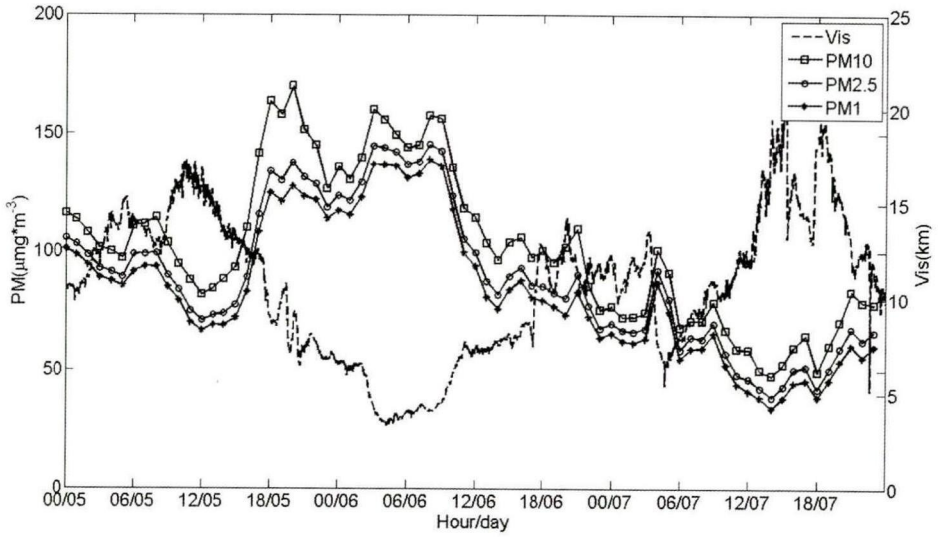

Figure 6. Variations of visibilities and atmospheric aerosol concentrations from 5 to 7, January 2014 at Dongguan observatory.

80% in this process, and aerosol moisture absorption growth was not apparent, so atmospheric visibility did not deteriorate, and minimum visibility was 4 km approximately. The percentage of $PM_{2.5}$ of PM_{10} was almost 80%, meaning the aerosol was dominated by fine particles.

According to the change in wind temperature profile and aerosol concentration shown in Figs.4 to 6 above, it can be seen clearly that the boundary layer structure has an apparent impact on aerosol concentration. From 6:00 to 8:00 on 5 January, the thermal inversion layer at the bottom boundary layer hindered pollutant dispersion, and then aerosol concentration increased to some extent, whereas the $PM_{2.5}$ concentration increased from 80 $\mu g \cdot m^{-3}$ to 110 $\mu g \cdot m^{-3}$. After the thermal inversion layer weakened and disappeared at 8:00 to 10:00, the $PM_{2.5}$ concentration decreased to 70 $\mu g \cdot m^{-3}$ as atmospheric diffusivity increased. From 12:00, due to the weak wind and calm wind on the boundary layer, as well as the limited horizontal diffusivity, the $PM_{2.5}$ concentration increased greatly; moreover, a stronger ground thermal inversion layer occurred in the afternoon of 5 January restricting the vertical diffusion of aerosol. After 18:00 on 5 January, this ground thermal inversion grew into a strong thermal inversion layer with a thickness of 500 m, causing a restriction to pollutant dispersion and a high aerosol concentration, where the PM_{10} and $PM_{2.5}$ concentration exceeded 150 $\mu g \cdot m^{-3}$ and 140 $\mu g \cdot m^{-3}$, respectively. After 10:00 on 6 January, this ground thermal inversion weakened and even gradually disappeared, so the $PM_{2.5}$ concentration decreased rapidly. On 7 January, the absence of a thermal inversion layer on the boundary layer and the higher wind force on the middle and high layers were beneficial to pollutant dispersion, and thence aerosol concentration was maintained at a lower level.

Figure 7 shows the trajectory chart of the sounding balloon on 5–7 January, 2014. According to Fig.7, the sounding balloon turned to the west and then the east at 8:00 on 5 and 6 January respectively; this vertical wind shear was not beneficial for aerosol transfer and dispersion. On 7 January, the sounding balloon moved uniformly to the northwest, which showed that airflow was stable and no pollutant accumulation occurred.

For surface aerosol concentration, atmospheric vertical diffusivity could have a direct impact on aerosol concentration when there is a stable local emission source. Within the atmospheric boundary layer, atmospheric vertical diffusion is mainly related to turbulent flow, but the thermal inversion layer could impose restrictions on the intensity of the turbulence. Fig.8 shows the air temperature at different heights varying with time on 5–7 January, 2014. According to Fig.8, it can be seen that air temperature from ground surface to 250 m tended to decrease rapidly after 18:00 on 5 January, which was related to the cold advection enhancement resulting from cold air, but it also might be caused by radiant temperature reduction on the other hand. Air temperature from 500 to 750 m increased slowly, and air temperature from 1 000 to 1 500 m also increased after 23:00, meaning that cold air activity occurred within a limited thickness and could reduce air temperature above 500 m, thus resulting in the ground thermal inversion. Air temperature in the high layer increased on the nights of 6 January and 7 respectively, but the temperature reduction speed from ground surface to 500 m was apparently lower than that of 5 January, and the intensity and thickness of the thermal inversion layer were smaller than those on 5 January.

For the ground surface, the ground thermal inversion layer can restrict the vertical diffusivity of aerosols, so the thickness and intensity of the ground thermal inversion layer (lapse-rate of air temperature) was closely related to aerosol concentration. Table 1 illustrates the

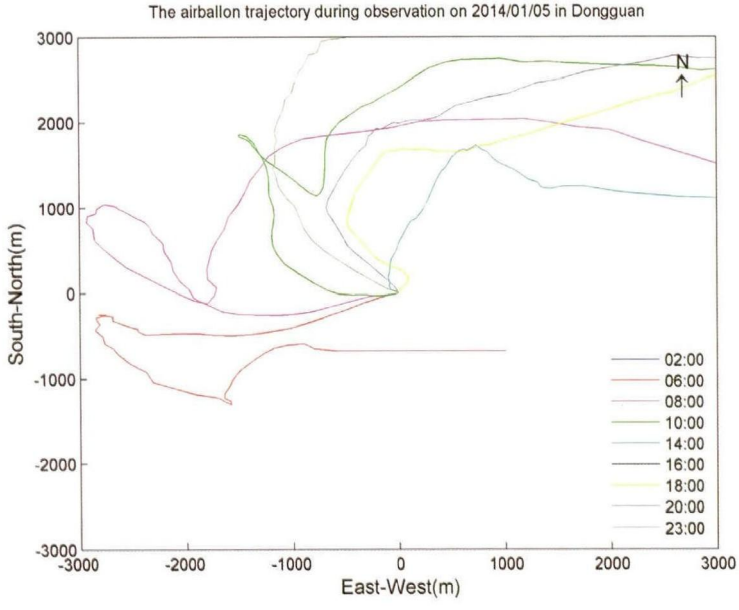

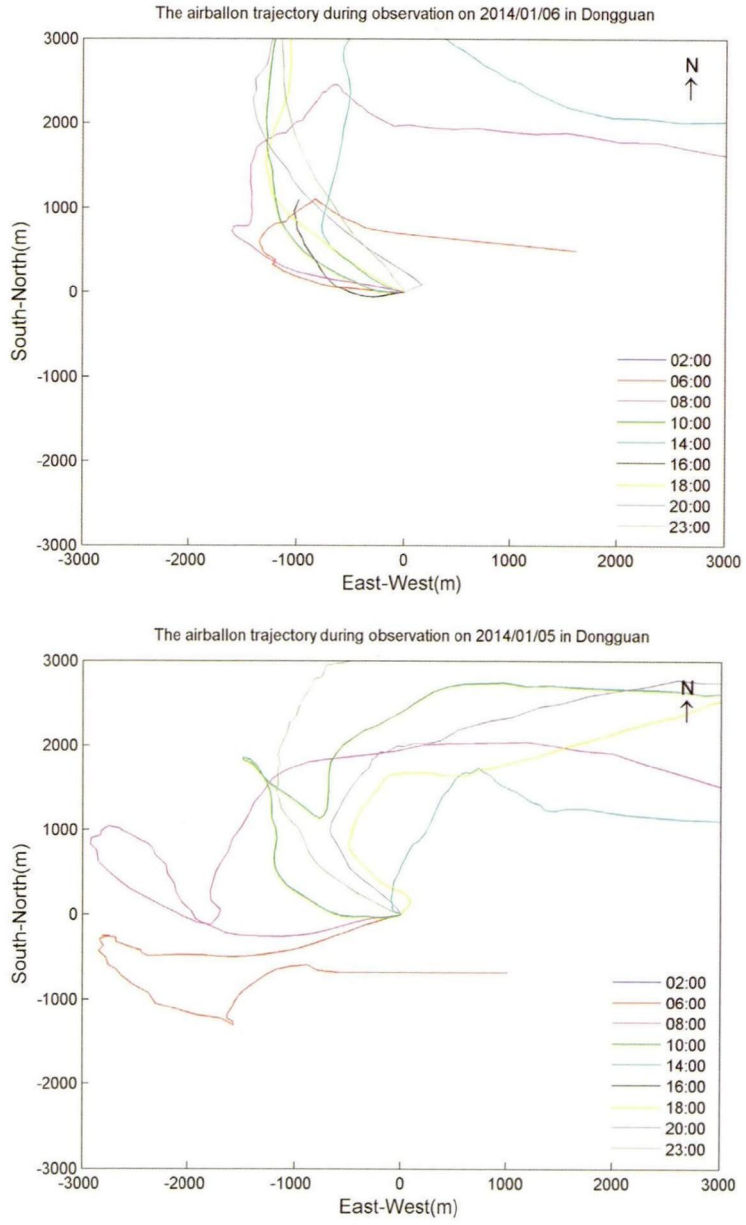

Figure 7. Balloon trajectories from 5 to 7, January 2014 at Dongguan observatory.

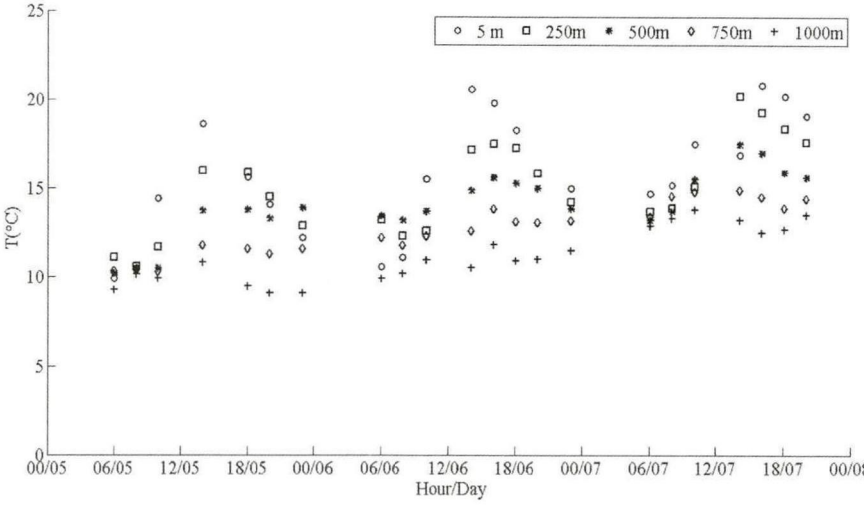

Figure 8. Variations of temperatures at different height from 5 to 6, January 2014 at Dongguan observatory.

Table 1. Thickness of the ground thermal inversion layer(m), average lapse-rate of air temperature on the ground thermal inversion layer(℃·m^{-1}) and the surface $PM_{2.5}$ concentration(μg·m^{-3}) on 5–7 January, 2014.

5 January	6:00	8:00	10:00	14:00	16:00	18:00	20:00	23:00
Ground thermal inversion layer	*	*				*	*	*
Thickness (m)	339	96				105	171	470
Average lapse-rate of air temperature (°C·m^{-1})	-4.13	-7.29				-15.24	-8.77	-4.26
$PM_{2.5}$ (μg·m^{-3})	98.66	99.12	83.75	73.68	89.03	133.68	137.45	118.52
6 January	6:00	8:00	10:00	14:00	16:00	18:00	20:00	23:00
Ground thermal inversion layer	*	*				*		*
Thickness(m)	512	529				96		123
Average lapse-rate of air temperature (°C·m^{-1})	-5.47	-4.16				-3.13		-8.13
$PM_{2.5}$ (μg·m^{-3})	136.5	145.07	123.26	81.48	93.19	85.25	80.11	67.33
7 January	6:00	8:00	10:00	14:00	16:00	18:00	20:00	23:00
Ground thermal inversion layer								
Thickness (m)								
Average lapse-rate of air temperature (°C·m^{-1})								
$PM_{2.5}$ (μg·m^{-3})	58.52	62.93	56.92	38.42	50.15	41.97	58.94	66.07

thickness of the ground thermal inversion layer, average lapse-rate of air temperature on the ground thermal inversion layer and the surface $PM_{2.5}$ concentration on 5–7 January, 2014. According to Table 1, ground thermal inversion was observed at 6:00, 8:00, 18:00, 20:00 and 23:00 on 5 January, and 6:00, 8:00, 18:00 and 23:00 on 6 January, which all occurred in the morning, at dusk or night. In most cases, the $PM_{2.5}$ concentration at the time when thermal inversion occurred was at a high level, namely 113.51 μg·m^{-3} on average and 145.07 μg·m^{-3} at the maximum. Contrarily, when the thermal inversion layer was absent, $PM_{2.5}$ concentration was 70.56 μg·m^{-3} on average. The thickness of the ground thermal inversion layer and lapse-rate of air temperature were related to the $PM_{2.5}$ concentration. All in all, the greater the thickness was, the higher the lapse-rate of air temperature was, and the higher the $PM_{2.5}$ concentration was. When the thickness of the ground thermal layer was 400 m or above, $PM_{2.5}$ concentration was always higher than 110 μg·m^{-3}.

4.2 *Impact of sea–land breeze shear line*

According the previous studies, the PRD region is often affected by sea-land breeze (Qiu and Fan [26]). Sea-land breeze occurs often on sunny days or in weather in which air temperature changes rapidly. The sea-land breeze convergence line, in addition to the vertical structure of the boundary layer, has significant influence on atmospheric aerosol dispersion.

Figure 9 shows the distribution diagram of wind direction and wind speed at the Dongguan Automatic Observation Station on 5 and 6 January, 2014. According to Fig.9, sea-land breezes tended to prevail in Dongguan on 5 and 6 January, 2014. Fig.8 shows the surface wind of Dongguan at 14:00 and 20:00 on 5 January and 6:00 and 14:00 on 6 January. According to Fig.8, it can be seen that the Dongguan Meteorological Station was in a weak surface shear line when sea breeze was at its highest at 14:00 on 5 January, whereas a dominant S-SE wind occurred to the south of the observation station, and the E or N wind field occurred to the north of the observation station, showing the ground of the region approaching the coastline was already affected by sea breeze. However, sea breeze in the vertical direction was not as high as 100 m and the scope of influence of the sea breeze was approximately 20 km away from the coastline, showing that its influence was at a low level. Sea breeze weakened significantly until 20:00 on 5 January, whereas the wind field weakened at 6:00 on 6 January, meaning that land breeze was not very apparent and the dominant wind field further decreased. The ground surface was under the control of the westward wind and the northwestward wind field was dominant to

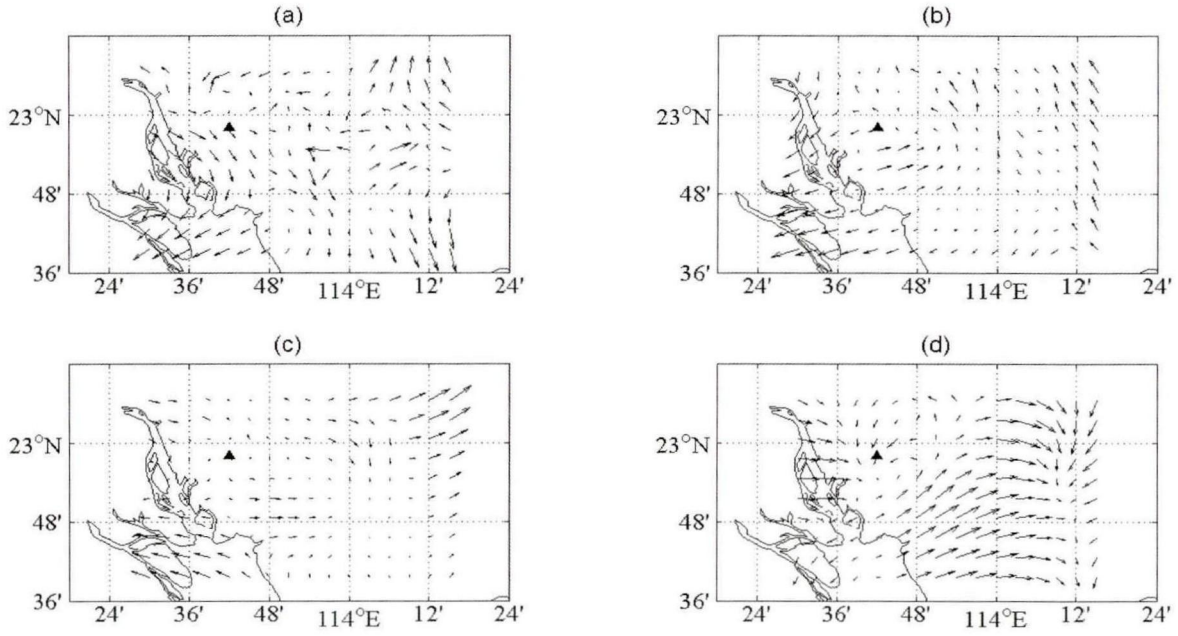

Figure 9. Surface wind from 5 to 6, January 2014 at Dongguan observatory. (a) 14:00 on 5 January, 2014; (b) 20:00 on 5 January, 2014; (c) 6:00 on 6 January, 2014; (d) 14:00 on 6 January, 2014.

the west by 14:00 on 6 January.

According to previous studies, sea-land breeze was not easily identified (Porson et al.[27]; Prtenjak[28]) when system wind was strong (more than 6 $m \cdot s^{-1}$). Among the individual cases studied in this paper, the PRD region was still controlled by a cold high pressure and under the influence of a northwestward system wind field, making land breeze hard to identify. However, the strength of sea breeze was higher than that of land breeze and the surface shear line or convergence line formed jointly by the sea breeze and the system wind were not beneficial for pollutant dispersion. According to the change in the direction and speed of the wind in the observation station (Fig.2), it can be seen clearly that an E- to NE-wind at the speed of approximately 3 $m \cdot s^{-1}$ was dominant before 14:00 on 5 January, but wind speed started decreasing after 14:00, and even decreased to 1 $m \cdot s^{-1}$ by 17:00. From 17:30, wind direction turned to the south and wind speed started increasing, which showed clearly the motion process of the shear line formed by the southward sea breeze and northeastward background wind, as well as its process of passing through the observation station. Sea breeze continued till 19:00, and weakened thereafter, and the direction of the wind at the observation station turned to the east. Meanwhile, aerosol concentration experienced a rapid increase at the observation station, which coincided with the duration of sea-land breeze shear line influence.

5 CONCLUSIONS

Through the analysis of the characteristics of the atmospheric boundary layer of Dongguan in winter and its impact on aerosol concentration, the following conclusions can be made:

In the late influence time of winter cold air, the cold high-pressure ridge and dominant system wind field weakened, causing horizontal atmospheric diffusivity to decrease. The surface layer of the boundary layer tended to be affected by local circulation, causing multilayer atmospheric boundary structure and imposing influence on atmospheric vertical diffusivity.

The boundary layer structure had very significant influence on surface aerosol concentration. The thermal inversion layer, especially the presence of strong ground thermal inversion, weakened atmospheric vertical diffusivity and interacted with the weak vertical shear of the wind to make surface aerosol concentration rise rapidly.

Thin cold air activity resulted in a ground thermal inversion layer, which was an important reason causing high surface aerosol concentration. In most cases, the $PM_{2.5}$ concentration was at a higher level when ground thermal inversion occurred, reaching 113.51 $\mu g \cdot m^{-3}$ on average and 145.07 $\mu g \cdot m^{-3}$ at the maximum. However, the $PM_{2.5}$ concentration was 70.56 $\mu g \cdot m^{-3}$ on average when no thermal inversion layer occurred. The thickness of the ground thermal inversion layer and lapse-rate of air temperature were related to $PM_{2.5}$ concentration. In general, the higher the thickness was, the higher the lapse-rate of air temperature was, and the higher the $PM_{2.5}$ concentration was.

With the influence of weak sea breeze, a southward wind field formed by sea breeze, associated with background wind, leads to a convergence line or weak

shear line, weakening atmospheric diffusivity. The resultant effect of the convergence line or weak shear line of the sea breeze and vertical thermal inversion layer of the atmosphere further weakened atmospheric diffusivity, causing a high aerosol concentration. The influence of the sea-land breeze shear line was a significant reason causing peak aerosol concentration.

REFERENCES:

[1] CHAN C, TANG J, LI Y, et al. Mixing ratios and sources of halocarbons in urban, semiurban and rural sites of the Pearl River Delta, South China [J]. Atmos Environ, 2006, 40: 7331-7345, doi:10.1016/j.atmosenv.2006.06.041.

[2] WU Dui, BI Xue-yan, DENG Xue-jiao, et al. Effect of atmospheric haze on the deterioration of visibility over the Pearl River Delta [J]. Acta Meteorol Sinica, 2007, 21: 215-223.

[3] CHEN Xun-lai, FAN Shao-jia, LI Jiang-nan, et al. Typical weather characteristics associated with air pollution in Hong Kong area [J]. J Trop Meteorol , 2008, 14: 101-104.

[4] FENG Y, WANG A, WU D, et al. The influence of tropical cyclone Melor on PM10 concentrations during an aerosol episode over the Pearl River Delta region of China: numerical modeling versus observational analysis [J]. Atmos Environ, 2007, 41: 4 349-4 365, doi:10.1016/j.atmosenv.2007.01.055.

[5] WU D, TIE X X, LI C C, et al. An extremely low visibility event over the Guangzhou region: a case study [J]. Atmos Environ, 2005, 39: 6 568-6 577, doi:10.1016/j.atmosenv.2005.07.061.

[6] XIA Dong, WU Zhi-quan, MO Wei-qiang, et al. Analysis of a Haze Process Caused by Peripheral Subsidence of Tropical Cyclones over the Pearl River Delta Region [J]. Meteorol Mon, 2013, 39 (6): 759-767, doi: 10.7519/j.issn. 1000-0526.2013.06.012.

[7] DING A J, WANG T, ZHAO M, et al. Simulation of sea-land breezes and a discussion of their implications on the transport of air pollution during a multiday ozone episode in the Pearl River Delta of China [J]. Atmos Environ, 2004, 38: 6 737-6 750, doi:10.1016/j.atmosenv. 2004.09.017.

[8] FAN Shao-jia, DONG Juan, GUO Lu-lu, et al. Analysis of the impact of urban growth on the tempreture field in Guangzhou [J]. J Trop Meteorol, 2006, 12: 24-28.

[9] DING A J, WANG T, XUE L K, et al. Transport of north China air pollution by midlatitude cyclones: case study of aircraft measurements in summer 2007 [J]. J Geophys Res, 2009, 114: D08304, doi:10.1029/2008jd011023.

[10] XIAO F, BRAJER V, MEAD R W. Blowing in the wind: the impact of China's Pearl River Delta on Hong Kong's air quality [J]. Sci Total Environ, 2006, 367: 96-111, doi: 10.1016/j.scitotenv.2006.01.010.

[11] CARRERAS H A, PIGNATA M L. Comparison among air pollutants, meteorological conditions and some chemical parameters in the transplanted lichen Usnea amblyoclada [J]. Environ Pollut, 2001, 111: 45-52.

[12] COGLIANI E. Air pollution forecast in cities by an air pollution index highly correlated with meteorological variables [J]. Atmos Environ, 2001, 35: 2 871-2 877.

[13] KHEDAIRIA S, KHADIR M T. Impact of clustered meteorological parameters on air pollutants concentrations in the region of Annaba, Algeria [J]. Atmos Res, 2012, 113: 89-101, doi:10.1016/j.atmosres.2012.05.002.

[14] TAN J H, DUAN J C, HE K B, et al. Chemical characteristics of PM2.5 during a typical haze episode in Guangzhou [J]. J Environ Sci, 2009, 21: 774-781, doi: 10.1016/s1001-0742(08)62340-2.

[15] MENUT, L, COLL I, CAUTENET S. Impact of meteorological data resolution on the forecasted ozone concentrations during the ESCOMPTE IOP2a and IOP2b [J]. Atmos Res, 2005, 74: 139-159, doi:10.1016/j.atmosres. 2004.04.008.

[16] GRINN-GOFRON A, STRZELCZAK A, WOLSKI T. The relationships between air pollutants, meteorological parameters and concentration of airborne fungal spores [J]. Environ Pollut, 2011, 159: 602-608, doi:10.1016/j.envpol.2010.10.002.

[17] KOLEV I, SAVOV P, KAPRIELOV B, et al. Lidar observation of the nocturnal boundary layer formation over Sofia, Bulgaria [J]. Atmos Environ, 2000, 34: 3 223-3 235.

[18] DAVIES F, MIDDLETON D R, BOZIER K E. Urban air pollution modeling and measurements of boundary layer height [J]. Atmos Environ, 2007, 41: 4 040-4 049, doi: 10.1016/j.atmosenv.2007.01.015.

[19] GAO Y, LIU X, ZHAO C, et al. Emission controls versus meteorological conditions in determining aerosol concentrations in Beijing during the 2008 Olympic Games [J]. Atmos Chem Phys, 2011, 11: 12437-12451, doi: 10.5194/acp-11-12437-2011.

[20] SCHLEICHER N, NORRA S, CHEN Y, et al. Efficiency of mitigation measures to reduce particulate air pollution-a case study during the Olympic Summer Games 2008 in Beijing, China [J]. Sci Total Environ, 2012, 427-428; 146-158, doi:10.1016/j.scitotenv.2012.04.004.

[21] ZHANG J P, ZHU T, ZHANG Q H, et al. The impact of circulation patterns on regional transport pathways and air quality over Beijing and its surroundings [J]. Atmos Chem Phys, 2012, 12: 5031-5053, doi: 10.5194/acp-12-5031- 2012.

[22] NEFF W, HELMIG D, GRACHEV A, et al. A study of boundary layer behavior associated with high NO concentrations at the South Pole using a minisodar, tethered balloon, and sonic anemometer[J]. Atmos Environ, 2008, 42: 2 762-2 779, doi:10.1016/j.atmosenv.2007.01.033.

[23] HANNA S R, MACDONALD C P, LILLY M, et al. Analysis of three years of boundary layer observations over the Gulf of Mexico and its shores, Estuar [J]. Coast Shelf S, 2006, 70: 541-550, doi:10.1016/j.ecss. 2006.06.005.

[24] EMEIS S, Mü NKEL C, VOGT S, et al. Atmospheric boundary-layer structure from simultaneous SODAR, RASS, and ceilometer measurements [J]. Atmos Environ, 2004, 38: 273-286, doi:10.1016/j.atmosenv.2003.09.054.

[25] ALAPPATTU D P, KUNHIKRISHNAN P K. Observations of the thermodynamic structure of marine atmospheric boundary layer over Bay of Bengal, Northern Indian Ocean and Arabian Sea during premonsoon period [J]. J Atmos Sol-Terr Phy, 2010, 72: 1 318-1 326, doi: 10.1016/j.jastp.2010.07.011.

[26] QIU Xiao-yuan, FAN Shao-jia. Progress of Sea Land Breeze Study and the Characteristics of Sea Land Breeze in Three Coastal Areas in China [J]. Meteorol Mon,

2013, 39 (2), 186-193, doi: 10.7519/j.issn. 1000-0526.2013.02.007.

[27] PORSON A, STEYN D, SCHAYES G. Formulation of an index for sea breezes in opposing winds [J]. J Climate Appl Meteor, 2007, 46: 1 257-1 263.

[28] PRTENJAK M. Main characteristics of sea/land breezes along the eastern coast of the Northern Adriatic [J]. Geofizika, 2003, 20: 75-92.

Citation: XIA Dong, FAN Shao-jia, LIAO Zhi-heng. Characteristics of boundary layer and its effects on atmospheric aerosol concentrations in Dongguan, Guangdong [J]. J Trop Meteorol, 2016, 22(1): 83-93.